J Mater Sci (2015) 50:4280–4287
DOI 10.1007/s10853-015-8980-6

Dinonylphenyl end-capped poly(ethylene glycol)-*b*-polystyrene: synthesis and its unusual crystalline and self-assembly behaviors

Hong Li[1] · Yijian Wu[1] · Yong Hu[1] · E. Bryan Coughlin[2] · Yongming Zhang[1]

Received: 3 January 2015 / Accepted: 17 March 2015 / Published online: 27 March 2015

Abstract Block copolymers, dinonylphenyl end-capped polyethylene glycol-*b*-polystyrene (DNPE-PEO-*b*-PSs) were synthesized in a one-step atom transfer radical polymerization (ATRP) of styrene. The PEO block in the DNPE-PEO-*b*-PS samples (volume fraction of PS: 66.8–93.2 %) was found to be amorphous, which contrasts with DNPE-PEO precursor, traditional methoxide end-capped polyethylene glycol-*b*-polystyrene (PEO-*b*-PS) and dinonylphenyl end-capped poly-(ethylene glycol)-*b*-poly(fluorinated methyl methacrylate)(DNPE-PEO-*b*-PFMAs). Meanwhile, DNPE-PEO-*b*-PSs display an intriguing self-assembly behavior in solution. Block copolymer particles with mesoporous internal structures are directly formed by self-assembly of DNPE-PEO-*b*-PS in tetrahydrofuran/water solutions. It is proposed that DNPE end group has an important effect on the crystallization of the block copolymers as well as their self-assembly behaviors in solution.

Electronic supplementary material The online version of this article (doi:10.1007/s10853-015-8980-6) contains supplementary material, which is available to authorized users.

✉ Hong Li
lh102@sjtu.edu.cn

✉ E. Bryan Coughlin
coughlin@mail.pse.umass.edu

✉ Yongming Zhang
ymzhang@sjtu.edu.cn

[1] School of Chemistry and Chemical Engineering, Shanghai Jiao Tong University, Shanghai 200240, China

[2] Department of Polymer Science and Engineering, University of Massachusetts Amherst, Amherst, MA 01003, USA

Introduction

Block copolymers are of great scientific interest due to their self-assembled supra-molecular structures in bulk or in solution. Generally, in bulk, block copolymers with immiscible blocks can microphase separate as a function of composition into the well-known morphologies including spheres, cylinders, bicontinuous gyroids, and lamellae [1]. On the other hand, amphiphilic block copolymers can self-assemble to form a variety of aggregate structures in dilute solutions where the solvent preferentially solvates one of the blocks [2]. Diverse morphologies have been obtained by amphiphilic block copolymers self-assembly in solution. The most common structures are simple spherical micelles, rods, and vesicles [3–5]. More complex aggregate structures have also been observed, such as complex micelles [6–8], block copolymer particles (BCPs) with phase-separation structures [9–14], and mesoporous BCPs [15, 16]. BCPs with mesoporous internal structure are useful for drug delivery systems, catalysis, and sensors [17–20].

Polyethylene glycol-*b*-polystyrene (PEO-*b*-PS) is one of the most studied amphiphilic block copolymers [21–24]. These studies concerned its crystallization, phase structure, and morphologies in bulk and nanostructure that resulted from self-assembly in solution. General PEO-*b*-PS could only form very regular micelles [3, 23, 24]. In this paper, an oleophilic dinonylphenyl end-group was introduced to PEO-*b*-PS resulting in a novel block copolymer dinonylphenyl end-group [dinonylphenyl end-capped polyethylene glycol-*b*-polystyrene (DNPE-PEO-*b*-PS)], which in some respect could mimic ABC triblock copolymers. Usually, the synthetic procedure of ABC block copolymers is challenging. At least two synthetic steps are required with two purification steps to obtain the final products. [25–30]. However, DNPE-PEO-*b*-PSs have been synthesized in

a one-step atom transfer radical polymerization (ATRP) of styrene using a commercially available nonionic alkyl poly(ethylene glycol) as starting material. We anticipate these new block copolymers have novel structure and properties compared with common PEO-*b*-PS due to the end-group effect. The end groups which are often ignored given their low weight fraction can have important effects on bulk crystallization of PEO and thermal phase transition temperature of PNIPAM [31–35]. However, the end-group effect on block copolymer is rarely reported. In this work, we investigated the bulk and solution behaviors of DNPE-PEO-*b*-PSs. Compared with commonly studied PEO-*b*-PS, DNPE-PEO-*b*-PS displays unusual crystalline behavior in bulk and self-assembly behavior in solution. The PEO block in the DNPE-PEO-*b*-PS samples (volume fraction of PS: 66.8–93.2 %) was found to be amorphous. BCPs with mesoporous internal structures are directly formed by self-assembly of DNPE-PEO-*b*-PS in tetrahydrofuran (THF)/water solutions. The size and structure of the BCPs change with water content. We expected that DNPE end groups play important roles in the morphological forming of DNPE-PEO-*b*-PS bulk and BCPs. This novel block copolymer with suppressed crystallization and the corresponding mesoporous BCPs could be interesting materials for catalysis, templating, delivery applications.

Experimental section

Materials

All commercially obtained solvents and reagents were used without further purification except as noted below. Polyethylene glycol dinonylphenyl ether (Igepal DM-970, Adlrich) (DNPE-PEO, $M_{n,MS} = 3896$ g/mol, $M_{n,NMR} = 3630$ g/mol, $M_{n,GPC} = 7900$ g/mol, $M_w/M_n = 1.05$) was washed with hexane, filtered, and dried in a vacuum oven. It was dissolved in anhydrous toluene and purified by azeotropic distilled before use. Styrene (St) was passed through a basic alumina column to remove the inhibitor before use. Dry toluene and THF were obtained by distilling over sodium (Na)/benzophenone. And dichloromethane (DCM) was distilled over calcium hydride (CaH_2) before use.

Preparation of DNPE-PEOBr macroinitiator

The procedure of preparation for DNPE-PEOBr macroinitiator was reported before [36]. Dry DNPEPEO (10 g, 3.0 mmol) and triethylamine (0.9 g, 9.0 mmol) were dissolved in dry DCM (75 mL). 2-Bromoisobutyrate bromide (13.7 g, 60 mmol) in DCM (25 mL) was added dropwise to the mixture at 0 °C. The mixture was stirred overnight at room temperature. The mixture was filtered and the solvent was removed by evaporation. The crude product was dissolved in THF and the solution was passed through a neutral alumina column. The macroinitiator DNPE-PEOBr was obtained in 78 % yield by precipitation from diethyl ether/petroleum ether (v/v 1/1). ($M_{n,NMR} = 3810$ g/mol, $M_{n,GPC} = 8100$ g/mol, $M_w/M_n = 1.08$).

Preparation of the block copolymer DNPE-PEO-*b*-PS

The synthesis of DNPE-PEO_{75}-*b*-PS_{107} is representative procedure: DNPE-PEOBr (0.9 g, 0.14 mmol), CuBr (0.020 g, 0.14 mmol), PMDETA (40 μL, 0.14 mmol), St (7.3 g, 189 mmol), and toluene (4 mL) were added to a Schlenk tube and subjected to three freeze–pump–thaw cycles, then heated for 20 h at 110 °C. Then copper catalyst was removed with a neutral alumina column. The product was obtained by precipitation from methanol. ($M_{n,GPC} = 24300$ g/mol, $M_{n,NMR} = 14770$ g/mol, $M_w/M_n = 1.19$).

Preparation of DNPE-PEO-*b*-PS BCPs

DNPE-PEO_{75}-*b*-PS_{218} was dissolved in THF. The solution was left standing at room temperature for one night and then filtered through a 0.45 μm PVDF membrane. Finally, different amounts of water were dropped into polymer solutions at designed temperatures under stirring.

Characterization

^{1}H NMR were taken on a Bruker DPX-300 NMR spectrometer in chloroform-*d* and dimethyl sulfoxide-d_6. Molecular weight and dispersity (Đ) were measured on an Agilent Technologies 1200 gel permeation chromatograph (GPC) in $CHCl_3$ at 40 °C with a flow rate of 1 mL/min on systems equipped with three-column sets (Polymer Laboratories 300 × 7.5 mm, 5 μm, 10–5, 10–4, and 10–3 Å pore sizes) and refractive index detectors (HP 1047A) at 40 °C. Polystyrene standards were used for molecular weight calibration. Matrix-assisted laser desorption ionization time-of-fight mass spectrometry (MALDI-TOF-MS) was performed on a Bruker Omniflex spectrometer equipped with a 337-nm nitrogen laser. 2,5-dihydroxybenzoic acid (DHB) was used as the matrix and sodium iodide (NaI) as the salt. Thermal behavior was analyzed by differential scanning calorimetry (DSC) using TA Instruments Q200 at a desired scanning rate under a flow of argon. Glass transition temperatures (*T*g) were determined as the midpoint of the transition process, and the exothermic and the endothermic maximum temperatures were taken as the crystallization temperatures

(Tc) and the melting temperatures (Tm), respectively. Dynamic light scattering (DLS) was performed on a high-performance particle sizer (Nano-ZS90, Malvern Instruments, UK) equipped with a He–Ne laser ($\lambda = 633$ nm) at a scattering angle $\theta = 90°$. Apparent mean hydrodynamic diameters D_h (according to volume distribution) of NPs were calculated according to Stokes–Einstein equation ($D_h = kT/3\pi\eta D_{app}$, with D_{app} and η being the apparent diffusion coefficient and viscosity of the solution, respectively). Scanning electron microscope (SEM) images of NPs on the silicon wafers were recorded using a NOVA NanoSEM 230. Transmission electron microscopy (TEM) images of NPs were observed on a JEM-2100 TEM operating at an acceleration voltage of 200 kV without any stain.

Results and discussion

Synthesis of block copolymers

The general synthetic procedure of the block copolymer DNPE-PEO-*b*-PSs is shown in Scheme 1. Firstly, dinonylphenyl end-capped polyethylene glycol macroinitiator (DNPE-PEOBr) was synthesized by a simple esterification reaction between the hydroxyl end groups in DNPE-PEO and 2-bromoisobutyryl bromide [36]. DNPE-PEO is a commercially available nonionic surfactant. The molecular weight and dispersity of DNPE-PEO before and after bromination are listed in Table 1. DNPE-PEOBr is an effective macroinitiator for ATRP of styrene. The chain length of the PS block can be controlled by varying the molar ratio of monomer/initiator and the polymerization time. Figure 1 shows the ^{1}H NMR spectrum of DNPE-PEO-*b*-PS. The characteristic resonance of the aromatic protons and methylene protons in the PEO block appeared at 6.2–7.4 ppm and 3.6 ppm, respectively, and their integrations can be calculated. The area of the aromatic protons in the DNPE end group is neglected since it is very small compared to that in PS block. So, according to the integrations of the aromatic protons and methylene protons as well as the molecular weight of DNPE-PEO, the $M_{n,NMR}$ of PS block was calculated. GPC traces of all samples in Fig. 2 are symmetric unimodal curves and shifted toward shorter elution time as compared with the macroinitiator. Block copolymers with PS block volume fraction ratios (f_{PS}) of 66.8–93.2 % were obtained. The characterization results are summarized in Table 1.

Crystalline behavior of PEO block

Polyethylene glycol (PEO) is a semicrystalline polymer, and its crystallization and melting behaviors have been studied in detail [37, 38]. Cheng et al. demonstrated the end-group dependence on crystallization behaviors of low-molecular weight PEO [39]. It was found that with increasing size of the end group, the thickening and thinning processes were increasingly hampered, but the crystal structure of the PEO with different end groups was identical. Here, the end-group effect on the crystallization of PEO block for DNPE-PEO-*b*-PS was studied. And the crystalline behavior of DNPE-PEO precursor, DNPE-PEO-*b*-PS, and PEO-*b*-PS was investigated by DSC. The sample was first heated from room temperature to 130 °C to eliminate thermal history, and then it was cooled from 130 to −80 °C and subsequently reheated to 130 °C at a rate of ±10 °C/min. The nonionic surfactant DNPE-PEO also shows a propensity for crystallization. The melting point (T_m) and crystallization point (T_c) of DNPE-PEO are around 55 and 40 °C, respectively (Supporting information, Fig. S1).

The degree of crystallinity for DNPE-PEO, X_c, calculated according to Eq. 1 is 73 %.

$$X_c = \Delta H_c/(f_{PEO} \times \Delta H_{f^0}), \quad (1)$$

where $\Delta H_{f^0} = 205$ J/g [40], which is the heat of fusion of 100 % crystalline PEO; f_{PEO} is the weight fraction of PEO in the polymer. However, all the DNPE-PEO-*b*-PS samples with PS volume fraction from 66.8 to 93.2 % did not show crystallization or melting points detected by DSC. Even when cooling and heating rate were reduced from 10 to 2 °C/min, no melting or crystallization peak appears in the DSC curve. (see Table 1 and Supporting Information, Fig. S2). For comparison, common methoxide end-capped poly(ethylene glycol-*b*-styrene)s (PEO_{114}-*b*-PS_{167} and PEO_{114}-*b*-PS_{244}) were synthesized by ATRP in our lab (Table 1). The PEO_{114}-*b*-PS_{167} has melting point at 35.9 °C with 10 % crystallinity and PEO_{114}-*b*-PS_{244} shows melting point at 33.6 °C with 30 % crystallinity, respectively, at the cooling and heat rates of 10 °C/min (also see

Scheme 1 Synthesis of DNPE-PEO-*b*-PS block copolymer

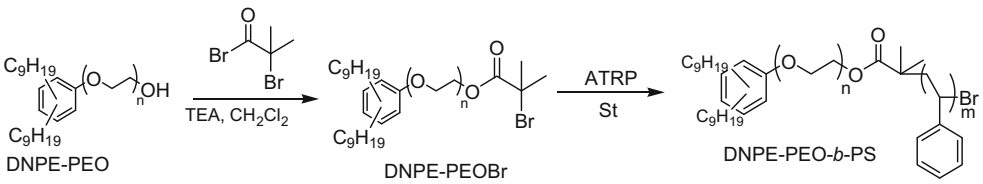

Table 1 Molecular characterization and thermal analysis of the DNPE-PEO-*b*-PS and MeOPEO-*b*-PS polymers and their precursors

Composition (NMR)	$M_{n,NMR}$	$M_{n,GPC}$	$Đ$	T_g^{PEO} (°C)	T_m^{PEO} (°C)	T_g^{PS} (°C)	f_{PS} (v%)*
DNPE-PEO_{75}	3630	7900	1.05	_	54.9		
DNPE-$PEOBr_{75}$	3810	8100	1.08	_	_		
DNPE-PEO_{75}-*b*-PS_{60}	9877	18300	1.18	-47.7	N	27.5	66.8
DNPE-PEO_{75}-*b*-PS_{90}	12905	19900	1.17	-46.7	N	31.1	75.1
DNPE-PEO_{75}-*b*-PS_{107}	14770	24300	1.19	-50.7	N	50.3	78.2
DNPE-PEO_{75}-*b*-PS_{132}	17289	23400	1.22	N	N	67.3	81.6
DNPE-PEO_{75}-*b*-PS_{170}	21283	28200	1.34	N	N	72.1	85.1
DNPE-PEO_{75}-*b*-PS_{409}	46166	51700	1.50	N	N	85.9	93.2
PEO	5000	9700	1.04	_	63.0		
PEOBr	5144	10500	1.04	_	_		
PEO_{114}-*b*-PS_{167}	22730	27800	1.15	–	34.1	57.8	78.7
PEO_{114}-*b*-PS_{244}	30376	37800	1.35	–	33.6	75.2	84.4

* Density of PEO and PS is 1.1210 and 1.0534 at 20 °C, respectively

N can not be detected

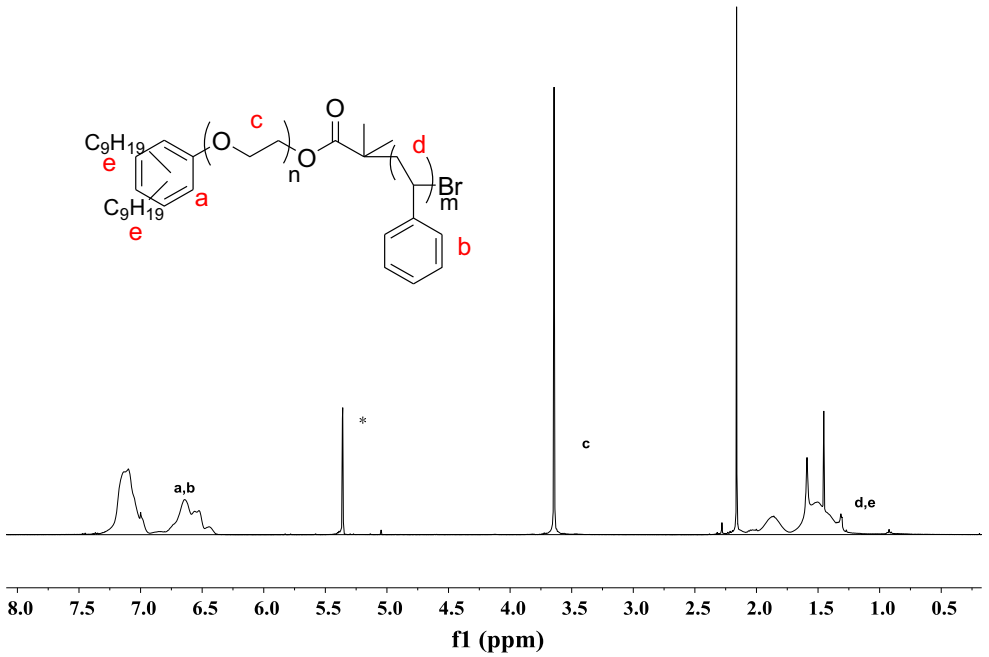

Fig. 1 ^{1}H NMR spectrum of DNPE-PEO-*b*-PS block copolymer in CD_2Cl_2

Supporting Information, Fig. S3). It is clear that crystallization of PEO in block copolymer is also end-group dependent. The end-group effect on crystallization of PEO-*b*-PS exceeds that on crystallization of homopolymer PEO. In latter case, end-group only has effect on the rate of the PEO crystallization, while DNPE makes crystallization of PEO in DNPE-PEO-*b*-PS completely suppressed. Interactions among DNPE groups, PEO block, and PS blocks may lead the copolymer to self-assemble in a morphology which suppresses the crystallization of PEO block entirely. Furthermore, our previous work demonstrated that PEO block in dinonylphenyl end-capped poly-(ethylene glycol)-*b*-poly(fluorinated methyl methacrylate) (DNPE-PEO-*b*-PFMAs) is semicrystalline [36]. The cylindrical morphology with PEO cylinders was confirmed for DNPE-PEO-*b*-PFMAs samples. The DNPE end-group does not mix with the fluoroacrylate segment so it has little effect on the crystallinity property of PEO block and microphase separation of the DNPEPEO-*b*-PFMAs. Based on comparison, we proposed that hydrophobic DNPE end-group in DNPE-PEO-*b*-PS may somehow tuck back into the hydrophobic PS phase, thus causing a loop or chain fold in the

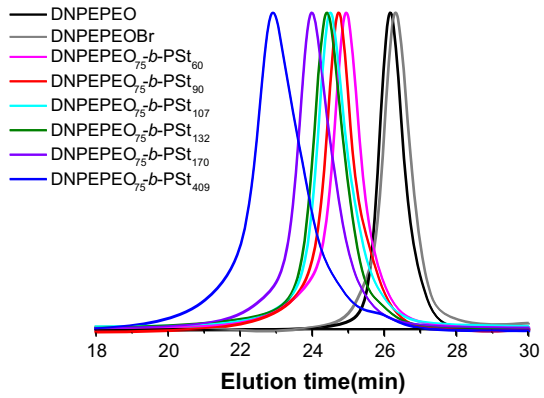

Fig. 2 GPC traces of DNPE-PEO, macroinitiator DNPE-PEOBr and DNPE-PEO-*b*-PS block copolymers

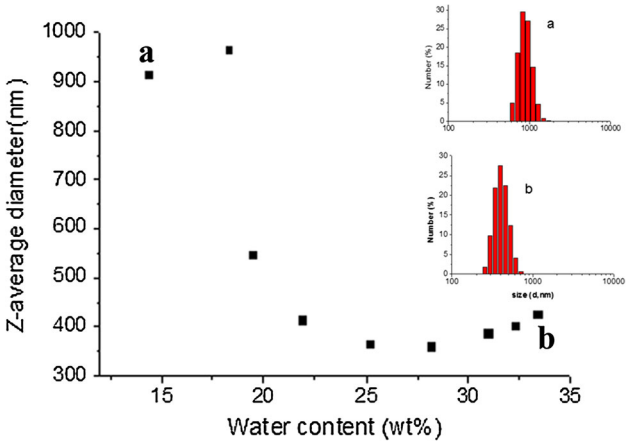

Fig. 3 The size of DNPE-PEO_{75}-*b*-PS_{409} BCPs changes with water content detected by DLS

PEO segment. This probably increases the chain entanglement effect on the crystallization and disrupts the PEO chain ability to crystallize.

Self-assembly in solution

Since DNPE-PEO-*b*-PS displays very unusual crystallization in bulk due to the end-group effect, it is worthwhile to study its self-assembly behavior in solution. Aggregate dispersions of the block copolymer DNPE-PEO_{75}-*b*-PS_{409} are formed by the addition of deionized water at a rate of about 10 μL/min while stirring in 0.1 wt% THF solution of the copolymer at 25 °C. The initial solutions went from transparent to light blue and white translucent during water addition, indicating aggregation of the copolymer during this process. DLS was applied to monitor the structure formation and transformation of the block copolymer aggregates. Measurement shows the size and distribution of the obtained BCPs changes greatly with the water content (Fig. 3). BCPs with the mean hydrodynamic diameters of 914 and 966 nm and polydispersity index (PDI) of 0.12 and 0.07 formed at the water content of 14.4 and 18.3 wt%, respectively. The measured average particle size is too large to correspond to the hydrodynamic diameters of normal spherical micelles as the contour length of the PS_{409} chain (~58 nm) so BCPs with fine internal structures might be formed. Size of the BCPs decreases when water content increases. As water content rises to 33.4 %, the size of the BCPs decreases to 425 nm with PDI of 0.05. Mechanism underlying the cause of size transformation of the BCPs with water content will be discussed later after microscopic studies.

The morphologies of these BCPs at different water contents were further investigated via TEM and SEM. According to Fig. 3, the morphology of the block copolymer aggregates depends quite sensitively on the water content, so, to reduce the effect of the water content on BCPs morphology as far as possible and to observe the transition morphology of the BCPs at different water contents, a direct evaporation of solvent method was applied to prepare TEM and SEM samples. In contrast to commonly used reprecipitation or dialysis method which can cause changes of the water content, for direct evaporation of solvent method, a small drop of the dispersion was placed directly on the carbon-coated copper grid or a silicon wafer. After solvents evaporate at room temperature, the BCPs on the copper grid or silicon wafer were observed by TEM or SEM. In this process, the solvent THF with a lower boiling point will evaporate more quickly at room temperature and residual selective solvent water can help to retain the morphology of the BCPs to a greater extent. Figure 4a shows spherical and elliptical BCPs formed at water content of 14.4 wt%. The size of the BCPs is quite dispersed. These BCPs exhibit internal cylindrical phase separated structure with darker block copolymer domains and gray/white solvent-filled channels. The width of the channels is about 15–25 nm. The cylindrical channels in such BCPs are with low order. Stacked toroids and distorted cylinders were observed. Figure 4b gives the SEM images of these BCPs. Many cracks were observed on BCPs surface.

Figure 5a shows both size and distribution of BCPs reduced and their internal cylindrical channels become compact on increasing the water content to 18.3 wt% at 25 °C, which may be attributed to extent of solvation of PS block and DNPE end-group reduced. Moreover, bicontinuous-like internal structures with a distinct dot pattern appeared in some large BCPs (Fig. 5a). As the water content increases to 25.2 %, the distribution of the BCPs become wider; meanwhile, their internal channels enlarged and the BCPs lost its regular spherical or elliptical shape (Fig. 5b).

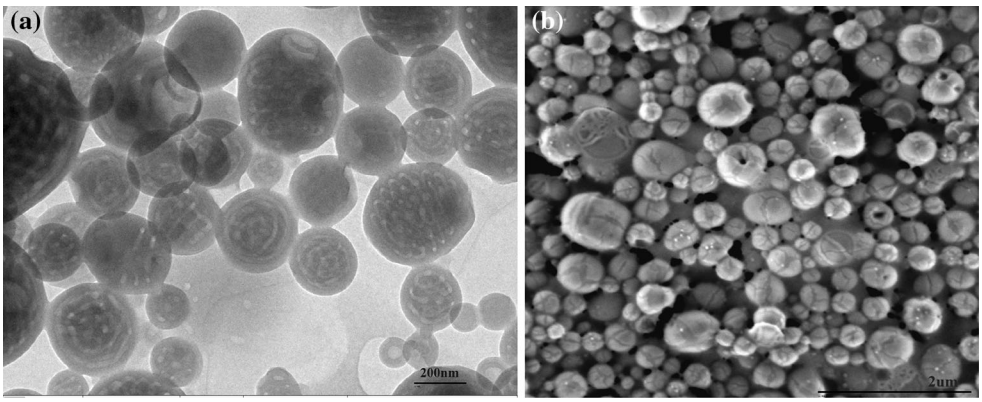

Fig. 4 Images of DNPE-PEO_{75}-*b*-PS_{409} BCPs prepared at 25 °C at water content of 14.4 wt% **a** TEM image, **b** SEM image

Further increasing the water content to 34 wt%, nanospheres with size of 100–200 nm are formed (Fig. 6a). The size of the BCPs shrinks to about half size of BCPs at the water content of 18.3 %, which agree well with DLS measurements. DLS studies show BCPs morphology in solvent, while common microscopic studies show BCPs morphology in dry state after evaporation of the solvent. They usually give different informations of BCPs. In our case, the particle size determined by DLS is much larger than that by TEM, but their variation trends of the particle size are consistent. The short porous phase in BCPs is quite vivid, mixing of toroid, sphere, short cylinder (distorted or not distorted, U-shape), two parallel short cylinders and a sphere in the inner layer with distorted cylinders in the outer layer. An interesting and rarely observed structure in the literature is a hollow sphere in the inner layer with cylinders in the outer layer (insets in Fig. 6a). This asymmetrical structure was only explored in diblock copolymers nanoparticles using real-space self-consistent field theory [41]. In addition, as shown in Fig. 6a, large particles have more complex internal structures than small particles, which revealed that the microphase separation structures in the nanoparticles are dependent on the diameters of the nanoparticles [16]. SEM image shows the obtained BCPs have completed and smooth surface (Fig. 6b), which might indicate this system arrived a certain quasi-equilibrium state.

According to the results of DLS and microscopic studies, we speculated that the whole process of the forming of the mesoporous BCPs and the mechanism underlying the course of size and shape transformation may be as follows: DNPE-PEO-*b*-PS started the self-assembly with water addition, since water is a poor solvent for PS block and DNPE end-group. For common PEO-*b*-PS, simple spherical micelles, rods, and vesicles will be obtained. However, for DNPE-PEO-*b*-PS, due to the immiscibility of PS/PEO parts and PEO/DNPE parts and favorable contact of DNPE with PS block, more complex aggregate structures occur. At lower water content, the polymer chains have enough mobility to form large BCPs with inner channels in solution. PEO block with water form a hydrophilic inner region and DNPE end-group and PS block close each other to form a hydrophobic outer region. The inner region can become trapped as THF evaporates, resulting in a channel structure [14]. Meanwhile, the morphology of the BCPs provides the interface limitation and geometric confinement for the microphase separation, so diverse internal structures within the BCPs were achieved. Increasing the

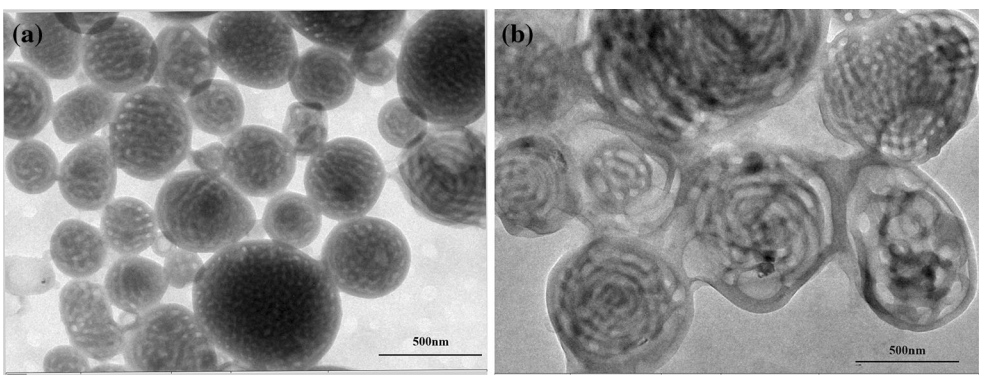

Fig. 5 TEM images of DNPE-PEO_{75}-*b*-PS_{409} prepared at water content of 18.3 wt% (**a**) and 25.2 wt% (**b**)

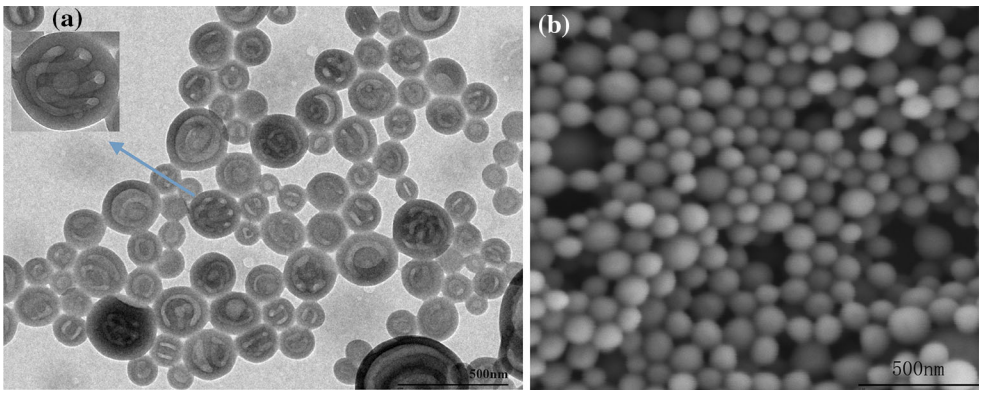

Fig. 6 Images of DNPE-PEO_{75}-*b*-PS_{409} BCPs prepared at water content of 34.0 wt% **a** TEM image, **b** SEM image

water content not only increased hydration of PEO block and the incompatibility among the three segments of the copolymer, but also reduced the chain mobility of the copolymer. As water content increases, their internal structure shrinks from long channel structures to short porous structures and outer structure also shrinks. The swollen PEO blocks collapse and much solvent was excluded from the channels, while the shrunk PS domain and DNPE group reconstruct new morphology with much smaller size. This happened due to greater hydration, which does not allow the larger BCPs to be held by the weakening hydrophobic environment [42, 43].

Conclusion

In summary, diblock copolymers with long-chain alkyl end-group (DNPE-PEO-*b*-PS) have been synthesized via ATRP of styrene using a commercially available surfactant. The block copolymers show intriguing crystalline and self-assembly behavior. The PEO block in all of the prepared DNPE-PEO-*b*-PS samples is amorphous, which contrasts with DNPE-PEO precursor, PEO-*b*-PS, and DNPEPEO-*b*-PFMAs. Morphology difference of these polymers is responsible for such phenomena. DLS measurements illustrate that by slowly adding water to DNPE-PEO_{75}-*b*-PS_{409} copolymer solutions in THF, the BCPs form complex micelle structures and the size and distribution of BCPs change greatly with water content. Observations by TEM and SEM illustrate that surface and internal structure of the BCPs changed with water content. At lower water content, BCPs with larger size have inner cylindrical channels structure and outer crackled surface. At higher water content, the inner structure transforms from cylindrical channels to short pores, and the surface become smoother. Interesting and uncommon structures such as bicontinuous-like and a hollow sphere in the inner layer with cylinders in the outer layer were observed. The internal mesoporous structures of the BCPs could be interesting materials for catalysis, templating, and delivery applications. And the related study is ongoing in our lab.

Acknowledgements We gratefully acknowledge funding for this work provided by the "12th 5-year" National Key Technologies R&D Program of China (2011BAE08B00), the Shanghai Natural Science Foundation (15ZR1422100), and State Key Laboratory of Hollow Fiber Membrane Materials and Processes (Tianjin Polytechnic University), Tianjin 300387, P. R. China. The authors thank the Instrumental Analysis Center, Shanghai Jiao Tong University for the SEM characterization.

References

1. Bates FS, Fredrickson GH (1999) Block copolymers—designer soft materials. Phys Today 52:32–38
2. Mai Y, Eisenberg A (2012) Self-assembly of block copolymers. Chem Soc Rev 41:5969–5985
3. Bhargava P, Zheng JX, Li P, Quirk RP, Harris FW, Cheng SZD (2006) Self-assembled polystyrene-block-poly(ethylene oxide) micelle morphologies in solution. Macromolecules 39:4880–4888
4. Jain S, Bates FS (2003) On the origins of morphological complexity in block copolymer surfactants. Science 300:460–464
5. Discher DE, Eisenberg A (2002) Polymer vesicles. Science 297:967–973
6. Zhong S, Cui H, Chen Z, Wooley KL, Pochan DJ (2008) Helix self-assembly through the coiling of cylindrical micelles. Soft Matter 4:90–93
7. Yu H, Jiang W (2009) Effect of shear flow on the formation of ring-shaped ABA amphiphilic triblock copolymer micelles. Macromolecules 42:3399–3404
8. Chen Z, Cui H, Hales K et al (2005) Unique toroidal morphology from composition and sequence control of triblock copolymers. J Am Chem Soc 127:8592–8593
9. Yamamoto T (2014) Molecular Dynamics of Crystallization in a Helical Polymer Isotactic Polypropylene from the Oriented Amorphous State. Macromolecules 47:3192–3202
10. Qin S, Li H, Yuan W, Zhang Y (2011) Hierarchical self-assembly of fluorine-containing diblock copolymer: from onion-like nanospheres to superstructured microspheres. Polymer 52:1191
11. Qin S, Li H, Yuan WZ, Zhang Y (2012) Fluorine-containing block copolymer particles with surface and internal hierarchical microphase separation structures. Soft Matter 8:2471–2476

12. Deng R, Liang F, Li W et al (2013) Self assembly: shaping functional nano-objects by 3D confined supramolecular assembly (small 24/2013). Small 9:4098–4098
13. McKenzie BE, Nudelman F, Bomans PHH, Holder SJ, Sommerdijk NAJM (2010) Temperature-responsive nanospheres with bicontinuous internal structures from a semicrystalline amphiphilic block copolymer. J Am Chem Soc 132:10256–10259
14. Hales K, Chen Z, Wooley KL, Pochan DJ (2008) Nanoparticles with tunable internal structure from triblock copolymers of PAA-*b*-PMA-*b*-PS. Nano Lett 8:2023–2026
15. Deng R, Liu S, Li J, Liao Y, Tao J, Zhu J (2012) Mesoporous block copolymer nanoparticles with tailored structures by hydrogen-bonding-assisted self-assembly. Adv Mater 24:1889–1893
16. Fan H, Jin Z (2014) Selective swelling of block copolymer nanoparticles: size, nanostructure, and composition. Macromolecules 47:2674–2681
17. Yang J, Lee C-H, Ko H-J et al (2007) Multifunctional magneto-polymeric nanohybrids for targeted detection and synergistic therapeutic effects on breast cancer. Angew Chem Int Ed 46:8836–8839
18. Lu Z, Liu G, Phillips H, Hill JM, Chang J, Kydd RA (2001) Palladium nanoparticle catalyst prepared in poly(acrylic acid)-lined channels of diblock copolymer microspheres. Nano Lett 1:683–687
19. Dorin RM, Sai H, Wiesner U (2013) Hierarchically porous materials from block copolymers. Chem Mater 26:339–347
20. Jackson EA, Hillmyer MA (2010) Nanoporous membranes derived from block copolymers: from drug delivery to water filtration. ACS Nano 4:3548–3553
21. Zhu L, Cheng SZD, Calhoun BH et al (2001) Phase structures and morphologies determined by self-organization, vitrification, and crystallization: confined crystallization in an ordered lamellar phase of PEO-*b*-PS diblock copolymer. Polymer 42:5829–5839
22. Zhu L, Huang P, Cheng SZD et al (2001) Dislocation-controlled perforated layer phase in a PEO-PS diblock copolymer. Phys Rev Lett 86:6030–6033
23. Kim KT, Zhu J, Meeuwissen SA et al (2010) Polymersome stomatocytes: controlled shape transformation in polymer vesicles. J Am Chem Soc 132:12522–12524
24. Yu K, Eisenberg A (1998) Bilayer morphologies of self-assembled crew-cut aggregates of amphiphilic PS-b-PEO diblock copolymers in solution. Macromolecules 31:3509–3518
25. Kyerematen SO, Amado E, Blume A, Kressler J (2008) Synthesis of ABC and CABAC triphilic block copolymers by ATRP combined with 'click' chemistry. Macromol Rapid Commun 29:1140–1146
26. Kyerematen SO, Busse K, Kohlbrecher J, Jr Kressler (2011) Synthesis and self-organization of poly(propylene oxide)-based amphiphilic and triphilic block copolymers. Macromolecules 44:583–593
27. Skrabania K, Laschewsky A, Hv Berlepsch, Böttcher C (2009) Synthesis and micellar self-assembly of ternary hydrophilic–lipophilic–fluorophilic block copolymers with a linear PEO chain. Langmuir 25:7594–7601
28. Marsat J-N, Heydenreich M, Kleinpeter E, Berlepsch HV, Böttcher C, Laschewsky A (2011) Self-assembly into multicompartment micelles and selective solubilization by hydrophilic–lipophilic–fluorophilic block copolymers. Macromolecules 44:2092–2105
29. Skrabania K, Hv Berlepsch, Böttcher C, Laschewsky A (2009) Synthesis of ternary, hydrophilic–lipophilic–fluorophilic block copolymers by consecutive RAFT polymerizations and their self-assembly into multicompartment micelles. Macromolecules 43:271–281
30. Berlepsch HV, Bottcher C, Skrabania K, Laschewsky A (2009) Complex domain architecture of multicompartment micelles from a linear ABC triblock copolymer revealed by cryogenic electron tomography. Chem Commun 17:2290–2292
31. Du J, Willcock H, Patterson JP, Portman I, O'Reilly RK (2011) Self-assembly of hydrophilic homopolymers: a matter of RAFT end groups. Small 7:2070–2080
32. Zhong XF, Eisenberg A (1994) Aggregation and critical micellization behavior of carboxylate-terminated monochelic polystyrene. Macromolecules 27:1751–1758
33. Yu X, Zhong S, Li X et al (2010) A giant surfactant of polystyrene-(carboxylic acid-functionalized polyhedral oligomeric silsesquioxane) amphiphile with highly stretched polystyrene tails in micellar assemblies. J Am Chem Soc 132:16741–16744
34. Changez M, Kang N-G, Lee CH, Lee J-S (2010) Reversible and pH-sensitive vesicles from amphiphilic homopolymer poly(2-(4-vinylphenyl)pyridine). Small 6:63–68
35. Furyk S, Zhang Y, Ortiz-Acosta D, Cremer PS, Bergbreiter DE (2006) Effects of end group polarity and molecular weight on the lower critical solution temperature of poly(N-isopropylacrylamide). J Polym Sci 44:1492–1501
36. Li H, Gu W, Li L, Zhang Y, Russell TP, Coughlin EB (2013) Synthesis of semicrystalline/fluorinated side-chain crystalline block copolymers and their bulk and thin film nanoordering. Macromolecules 46:3737–3745
37. Takahashi Y, Tadokoro H (1973) Structural studies of polyethers, (–(CH2)m–O–)nX. Crystal structure of poly(ethylene oxide). Macromolecules 6:672–675
38. Takahashi Y, Sumita I, Tadokoro H (1973) Structural studies of polyethers IX. Planar zigzag modification of poly(ethylene oxide). J Polym Sci 11:2113–2122
39. Cheng SZD, Wu SS, Chen J et al (1993) Isothermal thickening and thinning processes in low-molecular-weight poly(ethylene oxide) fractions crystallized from the melt 4. End-group dependence. Macromolecules 26:5105–5117
40. Kovacs AJ, Straupe C (1980) Isothermal growth, thickening and melting of poly(ethylene-oxide) single crystals in the bulk: III. Bilayer crystals and the effect of chain ends. J Cryst Growth 48:210–226
41. Li S, Chen P, Zhang L, Liang H (2011) Geometric frustration phases of diblock copolymers in nanoparticles. Langmuir 27:5081–5089
42. Singh V, Khullar P, Dave PN, Kaura A, Bakshi MS, Kaur G (2014) pH and thermo-responsive tetronic micelles for the synthesis of gold nanoparticles: effect of physiochemical aspects of tetronics. PCCP 16:4728–4739
43. Khullar P, Singh V, Mahal A, Kumar H, Kaur G, Bakshi MS (2013) Block copolymer micelles as nanoreactors for self-assembled morphologies of gold nanoparticles. J Phys Chem B 117:3028–3039